










Extraordinary two-dimensionality in the $S = 1/2$ spatially anisotropic triangular quantum magnet $\text{Cu}(1,3\text{-diaminopropane})\text{Cl}_2$ with modulated structure

R. Tarasenko ¹, O. Vinnik ¹, J. Šebesta ^{2,3}, D. Legut ^{2,4}, J. Chovan ², E. Čížmár ¹, J. Strečka ¹,
K. Karlová ¹, P. J. Baker ⁵, L. Kotvytska ¹, M. Orendáč ^{1,6} and A. Orendáčová ^{1,*}

¹*Institute of Physics, P. J. Šafárik University, Park Angelinum 9, 04001 Košice, Slovakia*

²*IT4Innovations, VSB-Technical University of Ostrava, 17. listopadu 2172/15, CZ 708 00 Ostrava-Poruba, Czech Republic*

³*Department of Physics and Astronomy, Uppsala University Box 516, 751 20 Uppsala, Sweden*

⁴*Department of Condensed Matter Physics, Faculty of Mathematics and Physics, Charles University, Ke Karlovu 3, 121 16 Prague 2, Czech Republic*

⁵*ISIS Pulsed Neutron and Muon Source, STFC Rutherford Appleton Lab, Harwell Campus, Didcot OX11 0QX, Oxon, England*

⁶*Department of Solid State Engineering, University of Chemistry and Technology, Technická 5, Prague 16628, Czech Republic*



(Received 5 May 2023; revised 21 November 2023; accepted 5 December 2023; published 28 December 2023)

The growth of sufficiently large single crystals of $\text{Cu}(tn)\text{Cl}_2$ ($tn=1,3$ -diaminopropane) enabled specific heat and susceptibility studies in various field orientations. The nearly invisible broad hump in zero-field specific heat at 0.6 K coincides with the change in the characteristic parameters of zero-field muon relaxation spectra. The lack of oscillations in the time spectra and their exponential character preserved down to 40 mK suggest the coexistence of static and fluctuating local fields associated with the prevalence of low-dimensional correlations. The extreme two-dimensionality is also manifested by the nonmonotonous character of the magnetic phase diagram. First-principle calculations of exchange couplings introduced a concept of a quasi-two-dimensional magnetic lattice with many couplings within the magnetic layers. The strongest ones lead to the model of a rectangular lattice with the intrachain coupling $J/k_B = 4.3$ K and the interchain coupling $J'/J = 0.46$, which provides excellent agreement with the zero-field specific heat. However, the susceptibility data suggest the importance of other weaker interactions in accord with first-principle studies. Significant broadening of field-induced specific heat anomalies may be ascribed to potential intrinsic partial magnetic disorder associated with the gradual modulation of tn positions in the crystal structure.

DOI: [10.1103/PhysRevB.108.214432](https://doi.org/10.1103/PhysRevB.108.214432)

I. INTRODUCTION

The model of the spin-1/2 Heisenberg antiferromagnet (HAF) on the square lattice with the nearest-neighbors (NN) coupling J became a paradigmatic model of low-dimensional magnetism [1]. Introducing spatial anisotropy and/or additional couplings leads to a variety of quantum states. The so-called J - J' model or spatially anisotropic triangular lattice which can be derived from the square lattice by adding one diagonal coupling J' , has been studied for many years [2–9]. The model interpolates between the chain ($J = 0$), triangular lattice ($J = J'$), and the square lattice ($J' = 0$). Most of the theoretical studies of the model have been focused on the quasi-one-dimensional region ($J'/J > 1$) due to the possibility of rich experimental response. The iconic Cs_2CuCl_4 compound with $J'/J \approx 3$ has become a famous candidate for the realization of the spin liquid state [10–12]. Theoretical studies of the magnetic phase diagram of the J - J' model in the one-dimensional limit revealed the stabilization of collinear antiferromagnetic order succeeded by spin density wave (SDW) and cone phases in higher magnetic fields [6]. Some deviations from the proposed theoretical diagram

observed in Cs_2CuCl_4 were ascribed to the effect of spin anisotropy and additional couplings [7]. Recently, an incommensurate SDW phase and its locking into an up-up-down magnetization plateau state was observed in Cs_2CoBr_4 , the $S' = 1/2$ spatially anisotropic triangular antiferromagnet [13].

Ground-state studies of the J - J' model in the two-dimensional region ($J'/J < 1$) found for $J'/J < 0.7$ stabilization of the collinear Néel order [2,3,14]. In this Néel phase the increase of the frustrated J' coupling leads to the gradual reduction of the order parameter down to zero value. As a result, for J'/J between 0.7 and 0.9, no magnetic order is expected [2,15]. First-principle studies of magnetic interactions in bis(ethylenedithio)-tetrathiafulvalene and $\text{Pd}(\text{dmit})_2$ salts [16,17] revealed that the ground states of these triangular magnets can be determined by additional effects (ring exchange, elastic coupling, second neighbor interaction) which become crucial if the J'/J ratio belongs to the interval 0.7–0.9. On the other hand, experimental studies [18,19] of $\text{Ba}_8\text{CoNb}_6\text{O}_{24}$ and $\text{Ba}_3\text{CoSb}_2\text{O}_9$ showed that the systems are close to the realization of a triangular magnet with $J'/J = 1$.

Theoretical studies of the generalized spatially anisotropic triangular lattice characterized by three different nearest-neighbor couplings J - J' - J'' revealed that the additional spatial anisotropy keeps the main features of the ground-state phase diagram of the J - J' model [20]. Besides that, the studies

*alzbeta.orendacova@upjs.sk

suggest that the separation of collinear and spiral order by a nonmagnetic phase seems to be a universal feature of frustrated two-dimensional systems with continuous symmetry [20]. Another modification of the J - J' model was theoretically investigated [21] by involving next-nearest-neighbor (NNN) coupling J_2 . The increase of the NNN coupling stabilizes Néel order while it reduces spiral order leaving room for spin liquid phases separating the Néel and spiral order. In the special case $J'/J = 1$, the involving NNN J_2 coupling leads to the appearance of gapless Dirac spin liquid [22]. However, as was shown in Ref. [23], the effect of inherent disorder in the triangular magnets can lead to the observation of spin liquid behavior. Recent experimental studies of the triangular Heisenberg magnet on the single-crystal $\text{Cu}_2(\text{OH})_3\text{NO}_3$ revealed the coexistence of short-range resonating valence bond correlations and long-range order as a result of many competing exchange interactions on the spatially anisotropic triangular lattice [24]. This study showed that structurally disorder-free magnetic materials with spatially anisotropic exchange interactions represent a possible arena for realization of spin liquid states.

Previous studies [25] of powdered $\text{Cu}(tn)\text{Cl}_2$ ($tn = \text{C}_3\text{H}_{10}\text{N}_2 = 1,3$ -diaminopropane) identified the compound as a candidate for the spin-1/2 HAF J - J' model with $J'/J < 0.6$. The effective intralayer coupling has been estimated $J_{\text{eff}}/k_B \sim 3$ K. The extreme weakness of interlayer interactions has been manifested by the absence of the specific heat λ -like anomaly associated with the phase transition to magnetic long-range order (LRO) down to 60 mK. The predominance of two-dimensional magnetic correlations at lowest temperatures become apparent in the quadratic dependence of low-temperature specific heat as well as in the reentrant character of magnetic phase diagram carrying features of Berezinskii-Kosterlitz-Thouless phase transition [25–27].

Recent thermodynamic and structural studies of $\text{Cu}(tn)\text{Cl}_2$ revealed a structural phase transition at about 160 K associated with the removing of the carbon disorder in tn rings present in the high-temperature phase with $Pnma$ symmetry. The low-temperature structure is characterized by modulation of tn rings with the symmetry of the $Pnma(0\beta 0)s00$ superspace group [28]. The growth of sufficiently large single crystals together with first-principle studies of a magnetic subsystem triggered further investigation of this unusual material. Present work involves single-crystal study of specific heat and susceptibility. The thermodynamic data are analyzed within magnetic models based on the results of first-principle calculations. The studies are completed by the spectra of muon spin relaxation. By combining these techniques, we can investigate the effects of many competing interactions in this triangular quantum magnet that manifest in significant suppression of interlayer correlations and preserve features of the two-dimensional behavior, even in the magnetically static low-temperature phase.

This paper is organized as follows. Experimental details are described in Sec. II. First-principle studies of exchange interactions and Monte Carlo simulations of finite-temperature properties of two-dimensional lattices are presented in Sec. III. Section IV is focused at the discussion of the strong two-dimensionality in $\text{Cu}(tn)\text{Cl}_2$ based on the analysis of experimental results including specific heat, susceptibility,

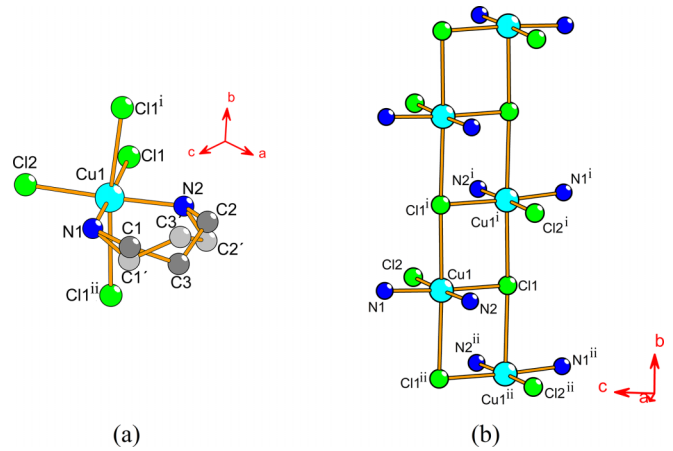


FIG. 1. (a) Drawing of the $\text{Cu}(tn)\text{Cl}_2$ molecule with two positions of tn ligand. Hydrogen atoms are omitted for clarity. (b) View of the ladderlike structure of $\text{Cu}(tn)\text{Cl}_2$ running along the crystallographic b axis. Hydrogen and carbon atoms are omitted for clarity.

and muon spin relaxation. The summary of results and some concluding remarks are presented in Sec. V.

II. EXPERIMENTAL DETAILS

The room-temperature structure is orthorhombic, space group $Pnma$, $a = 18.0056(5)$ Å, $b = 5.7572(2)$ Å, and $c = 6.9392(2)$ Å. Carbon atoms of tn rings are disordered over two positions related by a mirror plane [28] [Fig. 1(a)]. Such disorder was also observed in a similar compound [29] $\text{Cu}(en)\text{Cl}_2$ ($en = \text{C}_2\text{H}_8\text{N}_2 = \text{ethylenediamine}$) with monoclinic symmetry $P2_1/m$. Both materials are built of the same basic units: covalent zigzag $\text{Cu}(\text{II})$ ladders running along the b axis [Fig. 1(b)] and packed to a three-dimensional (3D) structure via a system of hydrogen bonds.

The structural phase transitions in both compounds did not influence the structure of ladders but led to the removing of the tn/en disorder. In $\text{Cu}(en)\text{Cl}_2$ the two different en configurations are homogeneously distributed occupying fixed positions in the separate legs of the ladders related to each other by the gliding operation, reflected by $P2_1/c$ symmetry [30]. The structural change in $\text{Cu}(tn)\text{Cl}_2$ was not so significant, which is also manifested by a much weaker and rather broad specific heat anomaly spreading through a temperature interval from 150 to 170 K [28]. Since the anomaly is very broad, previous structural studies at 150 K were able to catch only the features of the high-temperature phase which was described within the orthorhombic $Pna2_1$ symmetry [26] with the unit cell parameters $a = 17.9560(1)$ Å, $b = 6.8590(2)$ Å, and $c = 5.7100(5)$ Å. In this work the partial disorder in tn rings was characterized by two tn positions with occupancy factors 0.63 and 0.37. As was shown by recent studies [28], the transition in $\text{Cu}(tn)\text{Cl}_2$ occurs when the disordered high-temperature tn positions become modulated with two conformations. The low-temperature structure determined at 120 K is orthorhombic with unit cell parameters $a = 17.9290(7)$ Å, $b = 5.7022(5)$ Å, and $c = 6.881(2)$ Å, but with a modulation vector $q=0.1012b^*$ resulting in the

(3+1)-dimensional superspace group $Pnma(0\beta 0)s00$ (see Fig. S1 in the Supplement of Ref. [28]).

Following a method reported in Ref. [28], $\text{Cu}(tn)\text{Cl}_2$ single crystals were prepared in the form of blue-green flat plates with typical dimensions $a' \times b' \times c' = 2.5 \times 1.5 \times 0.5 \text{ mm}^3$. Using x-ray study the longest crystal edge a' was identified with the crystallographic b axis, the b' edge is parallel to the c axis, and the shortest crystal edge c' is parallel to the a axis.

Magnetic susceptibility measurements were performed in a commercial Quantum Design superconducting quantum interference device magnetometer equipped with a ^3He insert. Standard field-cooling (FC) and zero field-cooling (ZFC) regimes were applied. Samples with a typical mass of 0.2 mg were used for the bulk measurements. To increase the signal, temperature scans of magnetic moment were performed in the field $B(\equiv \mu_0 H)$ 0.5 T. The comparative data were recorded in analogical experiments with powdered samples with typical mass 50 mg to avoid errors introduced by tiny samples. Using standard Pascal constants, the susceptibility data were corrected for the core diamagnetism.

Specific heat measurements were performed using a commercial Quantum Design physical property measurement system equipped with a ^3He insert. The contribution of adenda was measured in separate runs. To exclude potential errors due to the low sample mass of single crystals, reference zero-field specific heat measurements were recorded on powdered samples pressed to pellets with mass 3 mg.

Muon spin relaxation (μSR) measurements were performed using the μSR instrument at the ISIS facility in a dilution refrigerator at temperatures from 40 mK up to 4 K in zero field and longitudinal magnetic fields up to 0.2 T. Pressed polycrystalline pellets were contacted onto a Ag plate with Apiezon N and covered in thin Ag foil, which was bolted to the cold finger. The thickness of the pellets was about 1.5 mm and the total weight of the sample was 3 g. The data were analyzed using the WIMDA program [31].

III. SPATIAL ANISOTROPY OF EXCHANGE COUPLINGS IN $\text{Cu}(tn)\text{Cl}_2$

A. First-principle studies

Incorporation of the aforementioned modulated structure into *ab initio* studies is not straightforward. Therefore, to catch the main features of the magnetic subsystem, we considered two distinct crystal structures (A and B) with $Pna2_1$ symmetry assuming no structural disorder in tn positions. In the first system denoted as A, all tn rings occupy one position of a chairlike conformation, which in Ref. [26] has occupancy factor 0.63. In structure B, all tn rings belong to the second position with the occupancy factor 0.37.

The electronic structures of both modified systems were obtained by density functional theory (DFT) calculations as implemented in the plane-wave based QUANTUM ESPRESSO (QE) suite [32,33], where the projector-augmented wave [34] pseudopotentials with electron exchange and correlation effects were treated by parametrized Perdew-Burke-Ernzerhof [35] approximation. The calculations were performed with a $(4 \times 10 \times 12)$ k mesh within the unit cell assuming a kinetic energy cutoff of 240 Ry for charge density and a 60 Ry cutoff

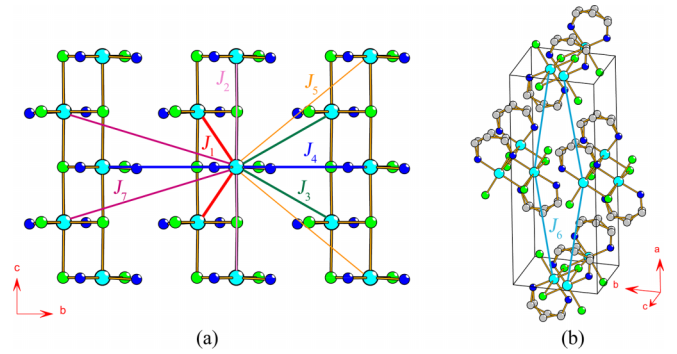


FIG. 2. (a) Exchange couplings within the bc magnetic layer determined for structure A. (Within the $Pna2_1$ symmetry the ladders run along the c axis; see text). Hydrogen and carbon atoms are omitted for clarity. (b) The interlayer coupling J_6 couples the bc layers. Hydrogen atoms and hydrogen bonds are omitted for clarity. The color code is the same as in Fig. 1.

for wave functions. van der Waals corrections of Grimme's DFT-D3 type [36] were included. The calculated electronic structures were used to evaluate the magnetic exchange interactions by means of maximally localized Wannier functions [37]. They were obtained by the WANNIER90 package [38,39] and its module implemented in QE. We assumed the projections on the Cu ($sp^3 d^2$; d_{xy} ; d_{xz} ; d_{yz}), Cl (sp^3), and N (sp^3) orbitals. Due to computational demands, the Wannierization was performed on a reduced $(3 \times 8 \times 8)$ Monkhorst-Pack k grid. Finally, the magnetic pair exchange interactions J_{ij} were evaluated by the TB2J PYTHON package [40] based on the Liechtenstein-Katsnelson-Antropov-Gubanov formalism [41,42]. First-principle studies revealed a minimal impact of spin-orbit coupling on the values of isotropic exchange interactions [43]. Therefore we employed collinear calculations without spin-orbit coupling $H = \sum_{i \neq j} J_{ij} \mathbf{e}_i \cdot \mathbf{e}_j$ providing isotropic exchange interactions J_{ij} , where \mathbf{e}_i represents the spin magnetization direction at the atomic site i . For the given A and B geometries electronic structure calculations were performed assuming ferromagnetically ordered Cu moments as well as several antiferromagnetic (AF) configurations. Significant magnetic moments are localized only on the Cu atoms, of $0.5 \mu_B$ (Bohr magneton), and on Cl atoms, of $0.1 \mu_B$, regardless of the structure, the latter being always ferromagnetically ordered with respect to the closest Cu atom. The calculations revealed that the A geometry is about 80 meV more stable than the B one irrespective of the magnetic structure.

Focusing on Cu atoms, we extracted dominant nearest-neighbor Cu-Cu pair exchange interactions, neglecting those smaller than $1 \mu\text{eV}$. For clarity, the exchange interactions were sorted by the radial distance and ascribed to nearest-neighbor atomic shells containing exactly two elements by symmetry. We considered 14 Cu NNs coupled to the central spin via seven different exchange pathways with corresponding exchange couplings J_1, \dots, J_7 . Twelve Cu atoms are within the same bc layer and two neighbors (1+1) are in the adjacent bc layers (Fig. 2).

For all tested ferromagnetic (FM) and AF configurations over the A and B structures, the largest couplings within the

TABLE I. Exchange couplings calculated for the A and B structures with FM spin configuration and corresponding distances between the central and NN spins. For clarity, the J/k_B values are rounded to two decimals.

J_i	J_i (meV)		$\frac{J_i}{k_B}$ (K)		$d(\text{Cu}_0 - \text{Cu}_i)(\text{\AA})$
	A	B	A	B	
J_1	0.0782	0.0306	0.91	0.36	3.588
J_2	0.0037	0.0017	0.04	0.02	5.710
J_3	0.0118	~ 0	0.14	~ 0	5.744
J_4	0.0392	0.0325	0.46	0.38	6.895
J_5	0.0018	0.0026	0.02	0.03	8.952
J_6	0.0244	0.0350	0.28	0.41	9.096
J_7	0.0024	0.0035	0.03	0.04	9.372

bc plane are provided by J_1 and J_4 while the rather large J_6 plays a role of interlayer interaction.

In the following text, the results related to a single unit cell where FM magnetic ordering in DFT calculations was applied, are discussed. Exchange interactions obtained for AF configurations are reported in the Supplemental Material [43].

The exchange couplings calculated for individual A and B structures are given in Table I. Here the central spin is localized on the Cu(II) ion denoted as Cu_0 while the NN spins are localized on the copper atoms denoted as Cu_i ($i = 1, \dots, 7$) with corresponding $\text{Cu}_0 - \text{Cu}_i$ distances. All exchange interactions are antiferromagnetic. As was already mentioned, nearly all exchange couplings are realized within the bc layer which can be treated as a magnetic layer [Fig. 2(a)]. There is only one interaction, J_6 , which acts between the bc layers [Fig. 2(b)].

To simplify the picture, first we will concentrate on the strongest coupling J_1 acting within the ladders forming the zigzag chains. From the magnetic point of view, they can be treated as linear antiferromagnetic Heisenberg chains with intrachain coupling J_1 . The chains are coupled via the second strongest coupling J_4 forming a rectangular lattice. Assuming the structure A, the third strongest intralayer coupling is J_3 acting along one diagonal of the $J_1 - J_4$ plaquette, thus forming a spatially anisotropic triangular lattice [Fig. 3(a)].

For completeness, much weaker coupling J_7 acts along the other diagonal of the aforementioned plaquette forming spatially anisotropic square lattice with two different diagonal couplings. When we return to the previous picture of the chain, then the coupling J_2 mediates the interaction between next-nearest neighbors within the chains. Concerning the weakest coupling J_5 , for clarity we can depict the distribution of the corresponding pathways on the separate Fig. 3(b). This interaction acts along one of the diagonals of the “superplaquette” created from two $J_1 - J_4$ plaquettes. The distribution of J_5 couplings forms a system of four penetrating square lattices.

Concerning structure B, the corresponding schema of the magnetic lattice is the same as in structure A, but without the J_3 coupling. Different values of exchange parameters calculated for both structures indicate the important role of tn configurations in the formation and effectivity of exchange pathways.

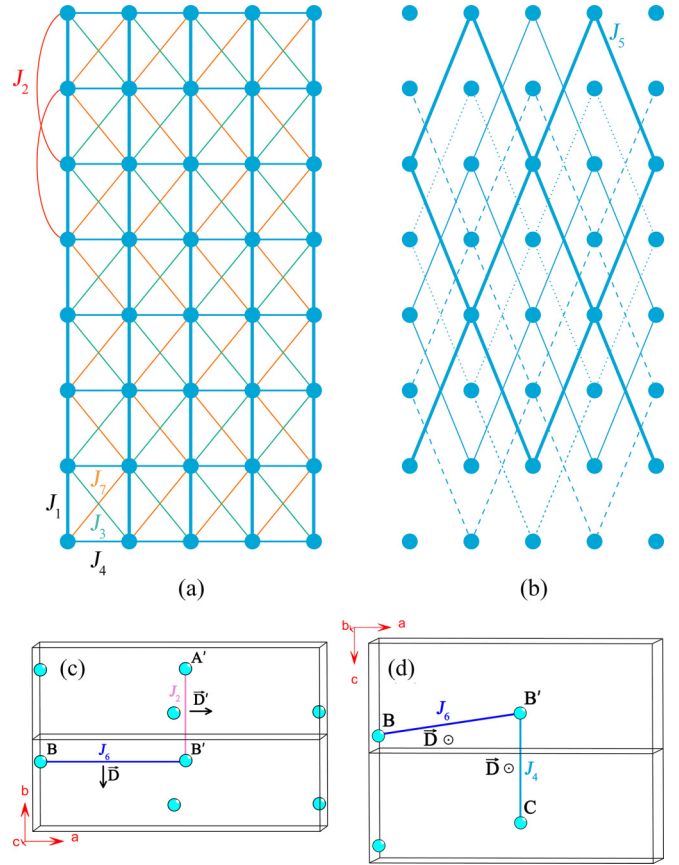


FIG. 3. (a) Schematic visualization of a magnetic lattice formed by exchange couplings within the bc plane. (b) The weakest intralayer coupling J_5 acts along one diagonal of the “superplaquette” formed by two plaquettes $J_1 - J_4$ depicted in Fig. 3(a). (c), (d) Dzyaloshinskii-Moriya vectors in the $\text{Cu}(tn)\text{Cl}_2$ structure allowed by the $Pnma$ symmetry. (Mirror plane parallel to the ac plane is perpendicular to the connector of A' and B' spins, and at the same time the connectors of B' and B spins and B' and C spins lie within the mirror plane.)

Since $\text{Cu}(tn)\text{Cl}_2$ is a spin-1/2 system with one unpaired electron in a nondegenerate orbital, it was shown [7] that the Dzyaloshinskii-Moriya (DM) coupling will be present on the bonds mediating exchange interactions. The description of the crystal structure within the $Pnma$ symmetry allows the existence of three sets of DM interactions distributed along the J_2 , J_4 , and J_6 couplings [Figs. 3(c) and 3(d)].

B. Quantum Monte Carlo calculations

The most simplified approximation of the two-dimensional (2D) magnetic lattice depicted in Fig. 3(a) is a rectangular lattice or a spatially anisotropic square lattice described by the spin-1/2 Heisenberg Hamiltonian

$$H = \left[J \sum_{i,j} S_i S_j + J' \sum_{k,l} S_k S_l \right] - g\mu_B B \sum_{i=1}^N S_i^z \quad (1)$$

The parameters J and J' are positive and stand for the antiferromagnetic intrachain and interchain exchange coupling, respectively. The ratio $r = J'/J$ ranges from 0 to 1. The

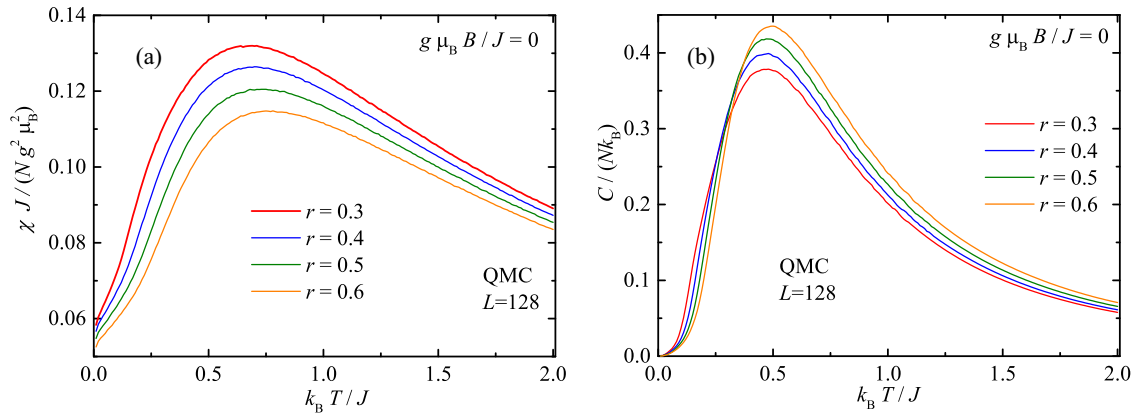


FIG. 4. Temperature dependence of the susceptibility (a) and specific heat (b) of the spin-1/2 HAF on the rectangular lattice in zero magnetic field calculated for r ranging between 0.3 and 0.6.

first and second summations involve the interaction between nearest neighbors within the chain and between the nearest neighbors from different chains, respectively. The third term in Eq. (1) is the standard Zeeman's term (g is Landé factor and μ_B is Bohr magneton). The calculations were realized using a directed loop algorithm in the stochastic series expansion representation of the quantum Monte Carlo (QMC) method [46] from the Algorithms and Libraries for Physics Simulations (ALPS) project [47]. The QMC simulations were performed on finite-size lattices with a linear size $L = 128$ spins, which involve under the periodic boundary conditions a total of $N = L \times L$ spins. The comparative studies with $L = 32$ and 64 found no finite-size effects. The adequate numerical accuracy was achieved through 10^6 Monte Carlo steps used for a statistical averaging in addition to 2.5×10^5 steps for thermalization. Partial calculations of thermodynamic properties of the model (1) can be found in the work [48]. For the requirements of the present analysis, corresponding calculations with finer r sampling were performed (Fig. 4).

IV. RESULTS AND DISCUSSION

A. Specific heat

Previous specific heat studies of polycrystalline materials in zero magnetic field were not able to detect any phase transition to a magnetically ordered state down to 60 mK [26]. On the other hand, a sharp λ -like anomaly was observed in the aforementioned $\text{Cu}(en)\text{Cl}_2$ single crystal at 0.7 K and the comparison of magnetic phase diagrams of both compounds suggested the potential phase transition also in $\text{Cu}(tn)\text{Cl}_2$ somewhere below 0.7 K [48].

Growing sufficiently large single crystals of $\text{Cu}(tn)\text{Cl}_2$ enabled specific heat studies. The material is an insulator, thus only magnetic and lattice subsystems contribute to the total specific heat. Magnetic specific heat C_{mag} in zero magnetic field was obtained after subtracting lattice contribution $C_{\text{latt}} = 2.43 \times 10^{-3} T^3 - 3.34 \times 10^{-6} T^5 + 2.59 \times 10^{-9} T^7$ estimated from a standard fitting procedure (Fig. 5). The local surrounding of the Cu(II) ion and 3D packing are nearly the same as in $\text{Cu}(en)\text{Cl}_2$ (Ref. [49]). Therefore, in the first approximation, we analyzed the magnetic specific heat data

within the model of spin-1/2 HAF on the rectangular lattice which was successfully applied for the description of the magnetic subsystem of $\text{Cu}(en)\text{Cl}_2$. Besides that, as was already mentioned in Sec. III A, first-principle calculations provide the two strongest couplings within the bc plane which form the rectangular lattice. Using the available numerical results reported in Ref. [48], the best agreement was found for $r = 0.4$ and 0.6 [Fig. 5(a)]. Apparently, the data are closer to the spatial anisotropy with $r = 0.4$. To improve the agreement, QMC calculations were performed for the ratios between 0.4 and 0.6 (Fig. 4). Finally, the best agreement with the data was achieved for $r = 0.46$ [Fig. 5(b)] with $J/k_B = 4.31$ K and $rJ/k_B = 1.98$ K. Apparently, the ratio of both NN couplings agrees well with the J_4/J_1 ratio calculated for the major position A (Table I). In this respect, the spatial anisotropy within the rectangular lattice estimated for $\text{Cu}(en)\text{Cl}_2$ is much stronger, $r = 0.2$, and intralayer couplings are much weaker, $J/k_B = 2.35$ K [48].

The comparison of low-temperature $\text{Cu}(tn)\text{Cl}_2$ experimental data with theoretical predictions depicted in the inset of Fig. 5(a) revealed a very weak and broad anomaly at about 0.60 ± 0.05 K which could be associated with the phase transition to a magnetic ordered state as deduced from the aforementioned comparison of magnetic phase diagrams [48]. As was shown in the work [50] the heat-capacity jump at the transition temperature T_C , $\Delta C_{\text{mag}}(T_C)$, is expected to be of order $[S_{\text{mag}}(T_C)/S_{\text{mag}}(\infty)](M/M_0)^2 \Delta C^{\text{MF}}$, where ΔC^{MF} is the mean-field value ($1.5R$). The quantities R , S_{mag} , and M/M_0 represent universal gas constant, magnetic entropy, and relative staggered magnetization, respectively. Using the previous estimate [26] of ultralow-temperature $\text{Cu}(tn)\text{Cl}_2$ specific heat $C_{\text{mag}} = 1.35T^2$ and current data, $S_{\text{mag}}(T_C)$ was evaluated [0.33 J/(K mol)]. Since for the spin 1/2, the maximal entropy $S_{\text{mag}}(\infty) = R \ln(2) = 5.763$ J/(K mol), the long-range correlations can remove less than 6% from total spin entropy. Such low contribution manifests extreme two-dimensionality of the studied system. Further using the value $(M/M_0)^2 \approx 0.3$ estimated for the HAF square lattice [51] ($r = 1$), the value $\Delta C_{\text{mag}}(T_C)$ was calculated to be about 0.2 J/(K mol). This estimate is about four times higher than the real height of the anomaly superposed on the two-dimensional background

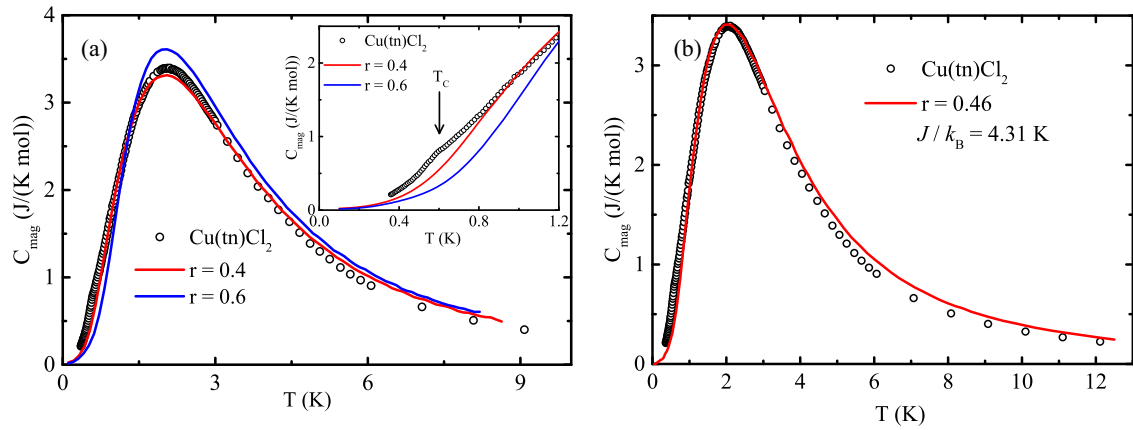


FIG. 5. (a) Temperature dependence of magnetic specific heat of a single-crystal $\text{Cu}(tn)\text{Cl}_2$ in zero magnetic field. The lines correspond to the $S = 1/2$ HAF model on the rectangular lattice with ratio $r = 0.4$ and 0.6 calculated in Ref. [48]. Inset: Zoom of the main plot at low temperatures. (b) The same experimental data as in (a); the line corresponds to the $S = 1/2$ HAF model on the rectangular lattice with $r = 0.46$ and $J/k_B = 4.31$ K.

which indicates much stronger reduction of the staggered magnetization. Theoretical studies of the $S = 1/2$ HAF on rectangular lattice [52,53] revealed a significant reduction of the order parameter only for $r < 0.2$. Apparently, the model of the rectangular lattice provides a very good description of zero-field specific heat within the region of short-range order [Fig. 5(b)], but the low-temperature anomaly potentially associated with the phase transition to magnetic long-range order reflects the effect of other 2D correlations.

The response of the sample in three different orientations of magnetic field is depicted in Fig. 6.

While along the b axis (parallel to ladders) only one anomaly is formed, along the other two directions the field induces two anomalies which merge in the field about 4 T. Despite the fact that all measurements were performed on single crystals, the induced anomalies are very broad. The analogous studies in $\text{Cu}(en)\text{Cl}_2$ indicated much sharper field-induced specific heat anomalies [48], similarly as in other quasi-2D $S = 1/2$ HAF $\text{Cu}(\text{II})$ based systems where the combination of a spatial and symmetric spin anisotropy led to the formation of simple reentrant magnetic phase diagrams with a spin-flop transition at lowest fields [54–56].

Concerning $\text{Cu}(tn)\text{Cl}_2$, the mapping of the anomalies provided a magnetic B - T phase diagram with a pronounced reentrant character manifesting weakness of interlayer interactions [Fig. 6(d)]. While in the field applied along the ladders, i.e., $\vec{B} \parallel b$, a simple one phase is observed, in the other two field orientations, $\vec{B} \perp b$, the diagram consists of two phases. The “high-temperature” phase is stable in the relatively narrow temperature interval in the vicinity of the critical temperature ~ 0.6 K and persists in the fields up to 4 T, which is about $2/3$ of the saturation field $B_{\text{sat}} \approx 6.5$ T estimated by previous powder studies [25]. At higher fields only one phase is stable. To find the origin of such behavior, the effect of spin anisotropies was theoretically investigated in Ref. [43], considering the high-temperature $Pnma$ symmetry.

The analysis of symmetric exchange anisotropies in $\text{Cu}(tn)\text{Cl}_2$ performed within the simplified two-sublattice model (Supplemental Material Fig. S1 in Ref. [43]) expects the formation of a noncollinear ground-state spin

configuration within the ac plane already in zero magnetic field if only the strongest intralayer couplings J_1 and J_4 are considered and the b axis is not the easy axis of the system [43]. In any case, the distribution of spin anisotropies guarantees that the development of the ground state under the application of magnetic field $\vec{B} \perp b$ differs from the situation when $\vec{B} \parallel b$. Concerning the DM interaction, the distribution of Dzyaloshinskii-Moriya vectors within the $Pnma$ symmetry [Figs. 3(c) and 3(d) and Figs. S6 and S7 in Ref. [43]] precludes the formation of helimagnetism within the bc plane due to much stronger intralayer antiferromagnetic coupling. On the other hand, the extremely weak interlayer coupling observed in the experiment prevents a DM interaction to induce spin canting between adjacent bc layers.

The present experimental data are not sufficient for the quantitative estimate of the symmetric spin anisotropies and DM interactions. As was shown in Ref. [43], the ground-state spin configuration depends on the hierarchy of the spin anisotropies, DM interactions, isotropic exchange interactions, and magnetic field. Thus, the determination of the resulting spin configuration even within the simplified two-sublattice model is beyond the scope of the present work.

The analysis of the low-temperature specific heat was performed in the fields opening a gap in the excitation spectrum $\Delta^{a,b,c} = g^{a,b,c} \mu_B (B - B_{\text{sat}}^{a,b,c})$ to estimate corresponding saturation fields. Assuming a predominantly 2D character of excitation spectrum, the data in 9 T were fitted by the relation [57] $C_{\text{mag}} \sim \exp(-\Delta/T)/T$. The fitting procedure provided field-induced gaps $\Delta^{a,b,c}/k_B = 3.4 \pm 0.2$ K, 4.9 ± 0.2 K, and 3.6 ± 0.2 K, respectively. Using $g^{a,b,c}$ factors 2.03, 2.25, and 2.05 taken from previous X-band electron paramagnetic resonance (EPR) studies [58], corresponding saturation fields $B_{\text{sat}}^{a,b,c} = 6.5 \pm 0.1$ T, 5.8 ± 0.1 T, and 6.4 ± 0.1 T were calculated from the aforementioned relation for the excitation gap $\Delta^{a,b,c}$. Then the saturation fields were included in the B - T diagrams at zero temperature [Fig. 6(d)]. These values were compared with saturation fields calculated within mean-field approximation for the $S = 1/2$ HAF on the rectangular lattice [48] $B_{\text{sat}}^{\text{2D}} = 2J(1+r)/(g\mu_B)$. Using the aforementioned $g^{a,b,c}$ factors and the parameters which provided a good

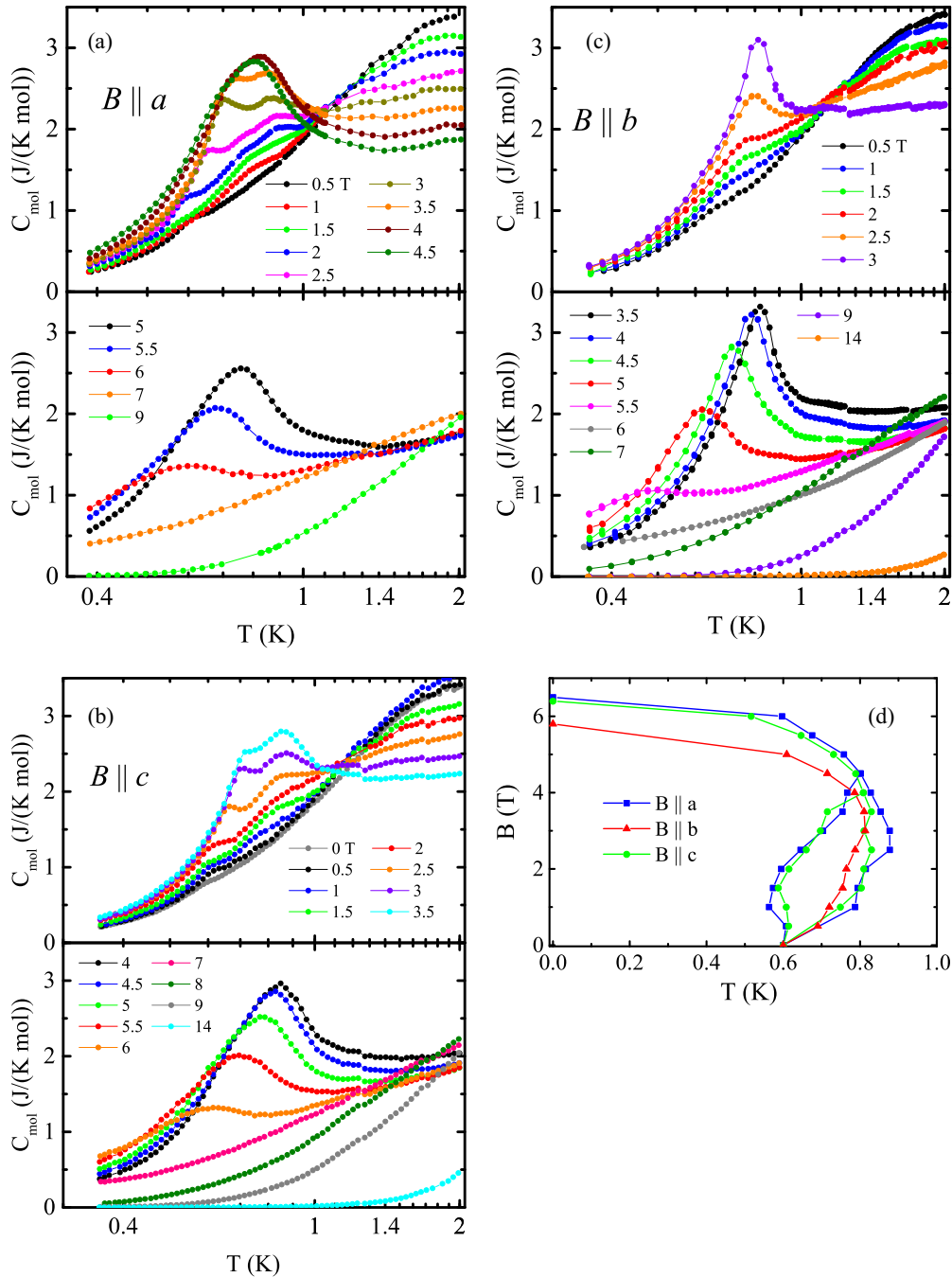


FIG. 6. Temperature dependence of specific heat of a single-crystal $\text{Cu}(tn)\text{Cl}_2$ in nonzero magnetic field applied along the a axis (a), c axis (b), and b axis (c). For clarity, only the temperature region of a field-induced anomaly is shown. (d) Magnetic phase diagrams along the a and c axes ($B \perp$ ladder) and b axis ($B \parallel$ ladder).

description of the experimental specific heat in zero magnetic field [Fig. 5(b)], the calculations yielded $B_{\text{sat}}^{\text{(rect)}}{}_{a,b,c} = 9.25, 8.34, \text{ and } 9.16$ T, respectively. Apparently, these 2D fields are much higher than the experimental values which contain also the contribution of interlayer couplings J' from z' neighbors in adjacent layers [59], $B_{\text{sat}} = B_{\text{sat}}^{\text{2D}} + z'J'/(g\mu_B)$.

Similarly, like the aforementioned significant reduction of the 3D anomaly at ~ 0.6 K in zero field [inset of Fig. 5(a)], the strong reduction of saturation fields suggests the influence of other competing interactions.

B. Susceptibility

The temperature dependence of magnetic moment was studied in the temperature range from 0.5 to 300 K in the field 0.5 T applied along the a , b , and c axes. The data obtained in the FC and ZFC regimes are identical. The corresponding single-crystal susceptibilities evaluated as $\chi = M/B$ together with the powder susceptibility are depicted in Fig. 7(a). The data in the field parallel to the ladders (b axis) show a sharp change at about 0.7 K. This temperature corresponds well to the field-induced transition temperature at 0.5 T as obtained

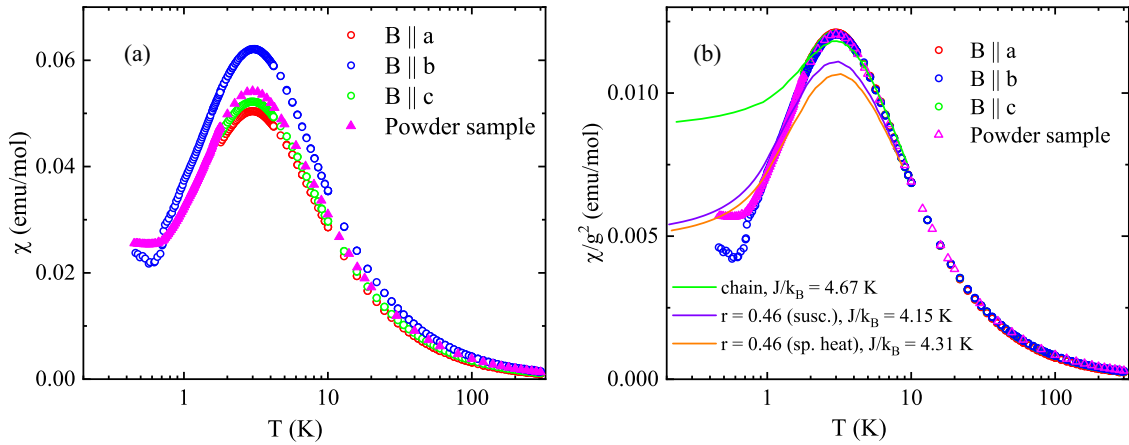


FIG. 7. (a) Temperature dependence of susceptibility of $\text{Cu}(tn)\text{Cl}_2$. (b) Temperature dependence of reduced susceptibility of $\text{Cu}(tn)\text{Cl}_2$ compared with corresponding predictions for the model of the $S = 1/2$ HAF chain and the rectangular lattice with $r = 0.46$.

from the specific heat anomaly [Fig. 6(d)]. No difference between FC and ZFC data below the phase transition indicates the absence of weak ferromagnetism in accord with the $Pnma$ symmetry. The rising tendency below the minimum at 0.6 K suggests that the b axis is not the easy axis as one would expect from the g -factor anisotropy.

Theoretical studies of finite-temperature properties of the $S = 1/2$ HAF on the square lattice revealed that the effect of the weak exchange anisotropy should appear at low temperatures $k_B T/J < 0.3$ while isotropic behavior is preserved at higher temperatures [60]. Therefore, to remove the effects of g -factor anisotropy, using the $g^{a,b,c}$ factors 2.05, 2.27, and 2.08, respectively, the temperature dependence of reduced susceptibility χ/g^2 was calculated to obtain a universal curve. The powder data were normalized by the average g value 2.12. The slight differences between the used g factors and those obtained from EPR result from the errors in the mass determination as well as in the possible deviations from the a , b , and c orientations during magnetic experiment. At temperatures above the phase transition all normalized data fall on the universal curve indicating g -factor anisotropy as the only source of the anisotropy in the paramagnetic phase [Fig. 7(b)]. Since the powder data were recorded in the field 0.1 T, the universal behavior excludes the nonlinear effects in low fields. The universal curve was compared with the corresponding prediction for the $S = 1/2$ HAF on the rectangular lattice with the parameters $r = 0.46$ and $J/k_B = 4.31$ K taken from the specific heat analysis.

The deviations from the model could not be suppressed by optimizing the J parameter for the position of the susceptibility maximum $T_{\max} = 3$ K for $r = 0.46$. Apparently, considering only the two strongest exchange couplings predicted by first-principle studies forming a rectangular lattice within the bc plane of $\text{Cu}(tn)\text{Cl}_2$ is not sufficient for the description of magnetic susceptibility [Fig. 7(b)].

Including J_3 , another strongest interaction within the bc plane [Fig. 2(a)], leads to the formation of the spatially anisotropic triangular lattice which can be described by the J - J' - J'' model. Besides the investigations of ground-state properties [20] we are not aware of finite-temperature studies of the model. Concerning the simpler J - J' model, high-temperature

series expansions were used to calculate the temperature dependence of susceptibility in the wide region of spatial anisotropies ranging from the square lattice to the chain limit [4]. This simplified model provided the best agreement for its chain limit, which contradicts the specific heat analysis. Apparently, the susceptibility is more sensitive to the onset and development of short-range correlations than to specific heat. While at temperatures above 3 K the experimental susceptibility data mimic one-dimensional (1D) behavior, at lower temperatures the influence of additional couplings becomes evident manifesting by the onset of huge deviations below 2 K, the temperature at which specific heat achieves maximum, corresponding to the largest changes of the internal energy.

C. μSR

ZF μSR experiments were performed on a polycrystalline sample at temperatures from 40 mK to 4 K. Over this temperature range we do not observe oscillations in the muon decay asymmetry spectra. The presence of oscillations would indicate the onset of long-range magnetic order. It should be noted that the oscillations were observed even in the quantum magnets with reported strong two-dimensionality [61,62]. Instead of the oscillations, in $\text{Cu}(tn)\text{Cl}_2$ the asymmetry spectra are intermediate between Gaussian and exponential forms at short times before a small recovery at longer times [Fig. 8(a)].

In the first step the raw data were fitted using the stretched exponential form of the muon relaxation $A(t) = A_{bg} e^{-\lambda_{bg} t} + A_0 e^{-(\lambda t)^\beta}$ with the background contribution involved. The fitting procedure provided nearly temperature independent baseline $A_{bg} \approx 5\%$ with $\lambda_{bg} \approx 0.02$ MHz, consistent with muons stopping in the Ag backing plate. The stretched exponent $\beta \approx 2$ was obtained in the temperature range from 4 K down to about 0.65 K indicating that muon spins are affected predominantly by the nuclear dipolar field from the surrounding nuclei. At lower temperatures the parameter β changes rapidly reaching $\beta \approx 1$ at lowest temperatures. Such change manifests the appearance of an additional component to the nuclear dipolar field originating from the Cu(II) electronic spin subsystem.

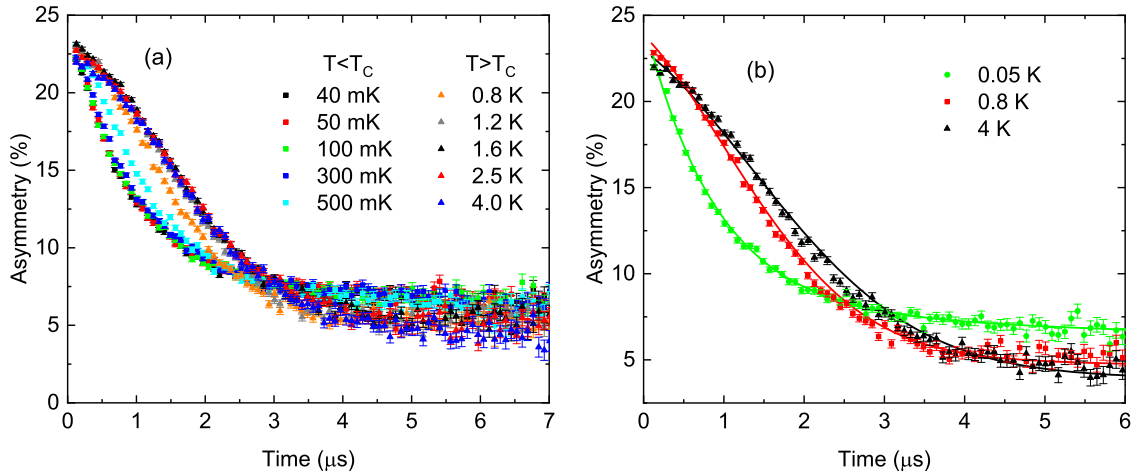


FIG. 8. (a) Zero-field μ SR spectra collected at various temperatures on the powdered sample of $\text{Cu}(tn)\text{Cl}_2$. (b) Examples of fitting the time spectra by Eq. (2). For clarity, only selected datasets are shown.

To separate the contribution of electronic and nuclear magnetic moments to the internal fields, the zero-field asymmetry curves were fitted with the relation [63,64]

$$A(t) = A_{\text{bg}} e^{-\lambda_{\text{bg}} t} + A_0 e^{-\lambda t} f_{\text{KT}}(\sigma, t), \quad (2)$$

where the second term is the product of two relaxation functions; f_{KT} is the static zero-field Kubo-Toyabe function $f_{\text{KT}}(\sigma, t) = \frac{1}{3} + \frac{2}{3}(1 - \sigma^2 t^2)e^{-(\sigma^2 t^2/2)}$ reflecting the Gaussian distribution of randomly oriented static local magnetic fields at the muon site arising from the nuclear spins. The parameter σ describes the width $\Delta = \frac{\sigma}{\gamma_\mu}$ of the Gaussian distribution and $\gamma_\mu = 8.516 \times 10^8 \text{ rad s}^{-1} \text{ T}^{-1}$ is the muon gyromagnetic ratio. The other part of the product represents the relaxation function arising from the dynamic magnetic fields generated by fluctuating Cu(II) electronic spins. The parameter λ is the muon spin relaxation rate associated with the fluctuating local fields of electronic spins. The multiplicative combination of two relaxation functions is due to the convolution of two field distributions, Gaussian and Lorentzian, which are primarily due to nuclear and electronic magnetic fields, respectively [63,64]. In the fitting by Eq. (2), the background parameter λ_{bg} was fixed using the values obtained from the fitting by stretched exponential form. Examples of the fitted spectra are shown in Fig. 8(b).

The fitting procedure provided the temperature dependence of the λ and σ parameters (Fig. 9). The behavior of λ is qualitatively the same as that obtained from the fit by the stretched exponential (not shown). As can be seen, the parameter $\sigma \cong 0.35 \text{ MHz}$ corresponds to $\Delta \cong 4 \text{ G}$ and is temperature independent down to 2 K. The observed value is typical for the relaxation governed by nuclear dipolar interaction [65]. The temperature 2 K coincides with the position of the round specific heat maximum (Fig. 5). At lower temperatures the parameter σ slightly grows achieving maximum 0.46 MHz ($\Delta \cong 5.3 \text{ G}$) at 0.57 K. This slight increase might be associated with the appearance of additional static fields resulting from the critical slowing down in the electronic spin subsystem. The sudden drop of σ below $\approx 0.57 \text{ K}$ coincides well with the rapid growth of λ . The fast change of both parameters suggests the phase transition at $0.57 \pm 0.05 \text{ K}$, which

corresponds to the appearance of the subtle wide hump in the specific heat [Fig. 5(a)].

Concerning the relaxation rate λ , in quasi-two-dimensional magnets above the phase transition this quantity reflects the behavior of 2D magnetic correlations characterized by the correlation length ξ_{2D} . As was shown in Ref. [65], the muon spin relaxation rate corresponds to the correlation length, $\lambda(T) \propto \xi_{2D}(T)$. Since the main features of 2D magnetism in $\text{Cu}(tn)\text{Cl}_2$ can be approximated by the rectangular lattice, the corresponding prediction for the correlation length [66] $\xi_{2D}(T) \propto \frac{e^{[2\pi\rho_s(r)/T]}}{(1+0.5\frac{T}{2\pi\rho_s(r)})}$ has been used for the fitting the relaxation rate. The spin stiffness ρ_s achieves maximal value $0.18J$ for the spatially isotropic square lattice ($r = 1$). Since the relaxation rate does not drop to zero values at higher temperatures, the fitting procedure was performed with some constant shift, $\lambda(T) = \xi_{2D}(T) + \lambda_0$. The best agreement was found for $2\pi\rho_s(r) = 1.9 \pm 0.15 \text{ K}$ and $\lambda_0 = 0.165 \text{ MHz}$ (Fig. 9).

At temperatures below 0.45 K the data deviate from the fitting curve probably due to the onset of long-range order. However, the static long-range order is not indicated in the

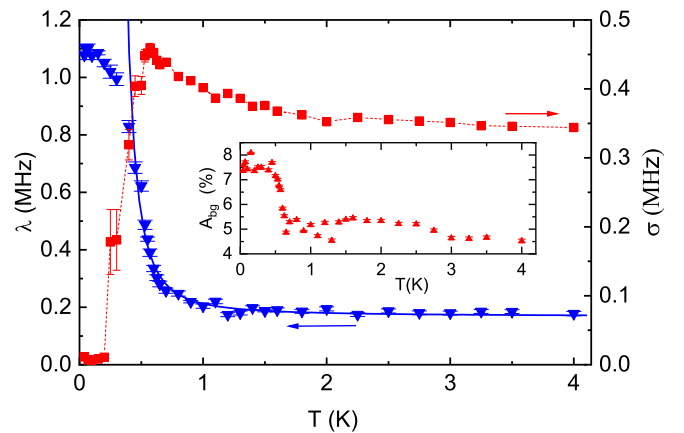
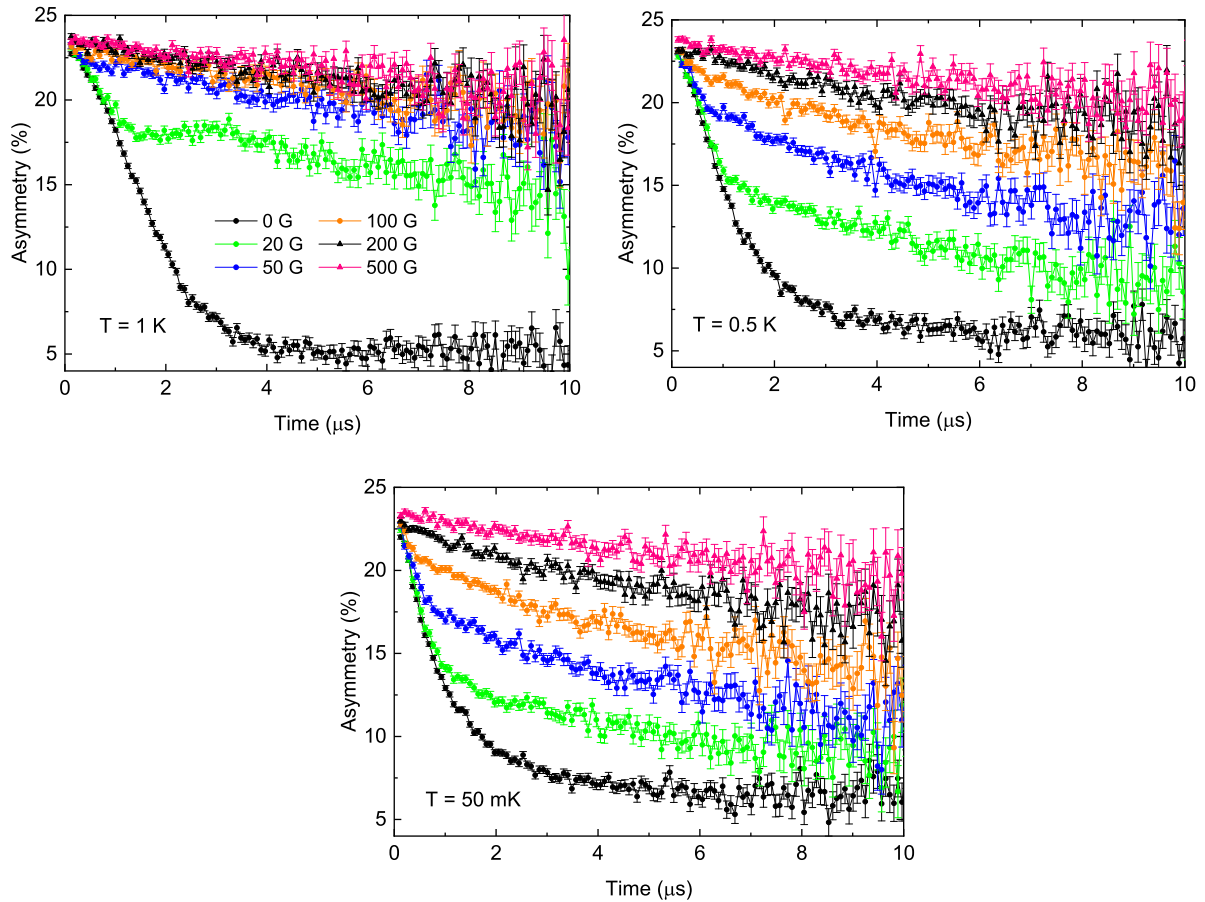


FIG. 9. Temperature dependence of the muon spin relaxation rate (triangles) and parameter σ (squares). The line represents the fit $\lambda(T) = \xi_{2D}(T) + \lambda_0$ (see text). Inset: Temperature dependence of the parameter A_{bg} [Eq. (2)] reflecting the behavior of the asymmetry baseline.

FIG. 10. LF μ SR spectra collected at various constant temperatures.

current muon spectra by characteristic oscillations of asymmetry. As was shown, the onset of LRO can be deduced only from the correlated changes of σ and λ parameters which coincide with subtle anomalies in specific heat and susceptibility. The corresponding local symmetry breaking in the magnetic fields the muons experience, results in the slight increase of the asymmetry baseline in the long time window at temperatures below 0.5 K (Fig. 8 and inset of Fig. 9). The main reason for such weak manifestation of LRO can be the prevalence of 2D correlations accompanied with the previously observed T^2 dependence of magnetic specific heat characteristic for good 2D magnets, persisting down to 60 mK [25–27].

Considering the paramagnetic phase, the value $2\pi\rho_s(r)$ obtained from the fitting of the relaxation rate represents about 50% reduction of $2\pi\rho_s(r=1) \approx 3.5$ K for the square lattice as a reference model. The average intralayer coupling $J_{av} = J(1+r)/2 \cong 3.1$ K was evaluated from the specific heat analysis within the rectangular lattice model for $r = 0.46$ while susceptibility suggests a more complicated model with a prevalence of 1D correlations and more than one sort of additional coupling within the magnetic layer (Figs. 5 and 7).

Theoretical studies of the J - J' model expect such strong reduction of the spin stiffness in the vicinity of the phase transition between Néel order and nonmagnetic ground state [3,14]. As for the effective rectangular lattice, the increasing spatial anisotropy towards 1D chains ($r \rightarrow 0$) leads to a strong

reduction of the spin stiffness ϱ_s^\perp in the direction perpendicular to chains while that along the chains ϱ_s^\parallel slightly increases above the reference square lattice value [53,67]. Using the ϱ_s^\parallel and ϱ_s^\perp values derived in Ref. [53] for $r = 0.4$ and 0.5 , the $\frac{\varrho_s^\perp}{\varrho_s^\parallel}$ ratio is between 0.2 and 0.3, which suggests rather weak interchain correlations within the magnetic layer. In this respect the fluctuations of weakly correlated chains could be treated as the main source of dynamically fluctuating local fields at low temperatures. As was shown in many theoretical studies, despite the prevalence of 1D correlations, such situation is completely different from a pure 1D case since even infinitesimal small interchain coupling can introduce 2D behavior.

The application of longitudinal field (LF) does not affect the width of distribution of randomly oriented static local magnetic fields at the muon site [68]. In the static case, the longitudinal field which is sufficient to decouple the muon spin from small static nuclear fields is in the order of distribution width Δ while in the dynamic case the magnitude of decoupling field is much larger [68,69]. Applying this criterion for distinguishing dynamic and static relaxation the LF μ SR experiments were performed above the phase transition at 1 K, in the vicinity of the phase transition at 0.5 K and far below the transition at 50 mK (Fig. 10).

While above the phase transition the longitudinal fields above 20 G can significantly flatten the muon time spectra

achieving decoupling of muons above $50\text{G} \sim 10\Delta$, the time spectra at 0.5 K show in this field significant relaxation. Finally, the spectra at 50 mK show decoupling in fields above $\sim 40\Delta$, which suggests dynamic relaxation due to fluctuating fields [68]. However, the aforementioned partial recovery of the asymmetry in long times in ZF spectra at 50 mK [Fig. 8(b)] points to some extent at the coexistence of static and dynamic random fields.

V. CONCLUSIONS

The growth of sufficiently large single crystals enabled the investigation of thermodynamic properties such as specific heat and susceptibility in various field orientations. Unlike previous polycrystalline studies, a nearly invisible broad hump in zero-field specific heat was observed and was ascribed to the onset of magnetic long-range order somewhere below 0.6 K. This observation coincides well with the behavior of the characteristic parameters of zero-field muon relaxation spectra. The lack of oscillations in the time spectra and the exponential character of the spectra preserved down to lowest temperatures suggest the coexistence of static order and fluctuating local fields associated with the strong influence of low-dimensional correlations. Their prevalence is also manifested by the previously observed T^2 dependence of specific heat far below the aforementioned phase transition and a nonmonotonous character of magnetic phase diagrams. Besides the reentrant behavior resulting from the strong magnetic two-dimensionality, the observation of an additional ordered phase appearing around the critical temperature in two field orientations calls for experimental studies of spin anisotropies which were already theoretically analyzed for $Pnma$ symmetry.

To understand the origin of the strong magnetic two-dimensionality, first-principle calculations of exchange couplings were performed based on the previously published assumption of two different positions of the 1,3-diaminopropane group in the structure. It was found that the tn positions strongly affect exchange interactions. The first-principle calculations introduced a concept of quasi-2D magnetic lattice in $\text{Cu}(tn)\text{Cl}_2$, comprising 2D arrays of magnetic chains with relatively strong intrachain coupling and many weaker interchain interactions spreading within the bc layer. The layers are coupled via a relatively strong interlayer interaction. Interestingly, the real interlayer coupling is a few orders of magnitude weaker than its theoretically predicted counterpart. This discrepancy may have its origin in the aforementioned use of approximate crystal structure with neglected modulation of tn position. Application of the quantum Monte Carlo technique enabled one to test the reliability of the first-principle predictions for the two strongest intralayer couplings presented by

the model of a rectangular lattice. While zero-field specific heat is in excellent agreement with the model of a rectangular lattice, its failure in the description of the susceptibility data suggests the importance of other weaker intralayer interactions. It should be mentioned that the current analysis of thermodynamic data suffered from the lack of theoretical predictions for more complicated 2D systems.

Apparently, $\text{Cu}(tn)\text{Cl}_2$ belongs to a few quantum magnets with extremely weak interlayer interactions of the order of dipolar coupling between nearly ordered magnetic layers. Unlike known examples in literature, the application of magnetic field leads to inducing of phase transitions which, despite monocrystalline samples, are accompanied with very broad specific heat anomalies. Since the exchange coupling parameters strongly depend on the position of the tn group, the observed broadening may be associated with the gradual modulation of tn positions in the structure leading to the decomposition of the lattice into many sublattices with more or less different exchange couplings. It can be a potential source of intrinsic partial magnetic disorder manifested in the muon relaxation spectra. Recently, various origins of the coexistence of the static a dynamic order have been reported, ranging from the unconventional character of the frustrated magnetic lattice with well-defined exchange constants [70] to the presence of structural defects [71]. $\text{Cu}(tn)\text{Cl}_2$ does not belong to any group since the structural disorder was already removed by the high-temperature structural phase transition and expected variability of exchange coupling parameters results from an intrinsic property of the perfectly ordered crystal structure. This conjecture calls for direct studies of magnetic ordering as well as for experiments clarifying the role of spin anisotropies in the ordering process in $\text{Cu}(tn)\text{Cl}_2$.

ACKNOWLEDGMENTS

This work has been supported by VEGA Grant No.1/0132/22 of the Scientific Grant Agency of the Ministry of Education, Science, Research and Sport of the Slovak Republic and the Slovak Academy of Sciences, Slovak Research and Development Agency Projects No. APVV-18-0197, GAČR projects 21-025505 and 22-35410K of the Grant Agency of Czech Republic, and projects of the Ministry of Education, Youth, and Sports of the Czech Republic, Grants No. LUASK22099, No. QM4ST CZ.02.01.01/00/22_008/0004572, and e-INFRA (ID:90140). In addition, J.S. acknowledges support from the Carl Trygger Foundation via Grant No. CTS20-153. Experiment RB1010054 “Investigation of magnetic order in the two-dimensional quantum magnet $\text{Cu}(tn)\text{Cl}_2$ ” at the ISIS Pulsed Neutron and Muon Source was supported by a beamtime allocation from the Science and Technology Facilities Council.

- [1] U. Schollwöck, J. Richter, D. J. J. Farnell, and R. F. Bishop, *Quantum Magnetism* (Springer, Berlin, 2004).
 [2] Z. Weihong, R. H. McKenzie, and R. R. P. Singh, Phase diagram for a class of spin-1/2 Heisenberg models interpolating between the square-lattice, the triangular-lattice, and the linear-chain limits, *Phys. Rev. B* **59**, 14367 (1999).

- [3] L. O. Manuel and H. A. Ceccatto, Magnetic and quantum disordered phases in triangular-lattice Heisenberg antiferromagnets, *Phys. Rev. B* **60**, 9489 (1999).
 [4] W. Zheng, R. R. P. Singh, R. H. McKenzie, and R. Coldea, Temperature dependence of the magnetic susceptibility for triangular-lattice antiferromagnets with spatially

- anisotropic exchange constants, *Phys. Rev. B* **71**, 134422 (2005).
- [5] M. Q. Weng, D. N. Sheng, Z. Y. Weng, and R. J. Bursill, Spin-liquid phase in an anisotropic triangular-lattice Heisenberg model: Exact diagonalization and density-matrix renormalization group calculations, *Phys. Rev. B* **74**, 012407 (2006).
- [6] O. A. Starykh and L. Balents, Ordering in spatially anisotropic triangular antiferromagnets, *Phys. Rev. Lett.* **98**, 077205 (2007).
- [7] O. A. Starykh, H. Katsura, and L. Balents, Extreme sensitivity of a frustrated quantum magnet: Cs_2CuCl_4 , *Phys. Rev. B* **82**, 014421(2010).
- [8] J. Reuther and R. Thomale, Functional renormalization group for the anisotropic triangular antiferromagnet, *Phys. Rev. B* **83**, 024402 (2011).
- [9] B. Schmidt and P. Thalmeier, Néel temperature and reentrant H - T phase diagram of quasi-two-dimensional frustrated magnets, *Phys. Rev. B* **96**, 214443 (2017).
- [10] R. Coldea, D. A. Tennant, A. M. Tsvelik, and Z. Tylczynski, Experimental realization of a 2D fractional quantum spin liquid, *Phys. Rev. Lett.* **86**, 1335 (2001).
- [11] C.-H. Chung, K. Voelker, and Y. B. Kim, Statistics of spinons in the spin-liquid phase of Cs_2CuCl_4 , *Phys. Rev. B* **68**, 094412 (2003).
- [12] Y. Tokiwa, T. Radu, R. Coldea, H. Wilhelm, Z. Tylczynski, and F. Steglich, Magnetic phase transitions in the two-dimensional frustrated quantum antiferromagnet Cs_2CuCl_4 , *Phys. Rev. B* **73**, 134414 (2006).
- [13] L. Facheris, K. Yu. Povarov, S. D. Nabi, D. G. Mazzone, J. Lass, B. Roessli, E. Ressouche, Z. Yan, S. Gvasaliya, and A. Zheludev, Spin density wave versus fractional magnetization plateau in a triangular antiferromagnet, *Phys. Rev. Lett.* **129**, 087201 (2022).
- [14] P. Hauke, T. Roscilde, V. Murg, J. Ignacio Cirac, and R. Schmied, Modified spin-wave theory with ordering vector optimization: Spatially anisotropic triangular lattice and $J_1 J_2 J_3$ model with Heisenberg interactions, *New J. Phys.* **13**, 075017 (2011).
- [15] E. Ghorbani, L. F. Tocchio, and F. Becca, Variational wave functions for the $S = 1/2$ Heisenberg model on the anisotropic triangular lattice: Spin liquids and spiral orders, *Phys. Rev. B* **93**, 085111 (2016).
- [16] E. P. Scriven and B. J. Powell, Geometrical frustration in the spin liquid β' - $\text{Me}_3\text{EtSb}[\text{Pd}(\text{dmit})_2]_2$ and the valence-bond solid $\text{Me}_3\text{EtP}[\text{Pd}(\text{dmit})_2]_2$, *Phys. Rev. Lett.* **109**, 097206 (2012).
- [17] R. V. Mishmash, J. R. Garrison, S. Bieri, and C. Xu, Theory of a competitive spin liquid state for weak Mott insulators on the triangular lattice, *Phys. Rev. Lett.* **111**, 157203 (2013).
- [18] R. Rawl, L. Ge, H. Agrawal, Y. Kamiya, C. R. Dela Cruz, N. P. Butch, X. F. Sun, M. Lee, E. S. Choi, J. Oitmaa, C. D. Batista, M. Mourigal, H. D. Zhou, and J. Ma, $\text{Ba}_8\text{CoNb}_6\text{O}_{24}$: A spin-1/2 triangular-lattice Heisenberg antiferromagnet in the two-dimensional limit, *Phys. Rev. B* **95**, 060412(R) (2017).
- [19] R. Chi, Y. Liu, Y. Wan, H.-J. Liao, and T. Xiang, Spin excitation spectra of anisotropic spin-1/2 triangular lattice Heisenberg antiferromagnets, *Phys. Rev. Lett.* **129**, 227201 (2022).
- [20] P. Hauke, Quantum disorder in the spatially completely anisotropic triangular lattice, *Phys. Rev. B* **87**, 014415 (2013).
- [21] M. G. Gonzalez, E. A. Ghioldi, C. J. Gazza, L. O. Manuel, and A. E. Trumper, Interplay between spatial anisotropy and next-nearest-neighbor exchange interactions in the triangular Heisenberg model, *Phys. Rev. B* **102**, 224410 (2020).
- [22] S. Hu, W. Zhu, S. Eggert, and Y.-C. He, Dirac spin liquid on the spin-1/2 triangular Heisenberg antiferromagnet, *Phys. Rev. Lett.* **123**, 207203 (2019).
- [23] Z. Zhu, P. A. Maksimov, S. R. White, and A. L. Chernyshev, Disorder-induced mimicry of a spin liquid in YbMgGaO_4 , *Phys. Rev. Lett.* **119**, 157201 (2017).
- [24] L. Yuan, Y. Zhao, B. Li, Y. Song, Y. Xia, B. Liu, J. Wang, and Y. Li, Possible coexistence of short-range resonating valence bond and long-range stripe correlations in the spatially anisotropic triangular-lattice quantum magnet $\text{Cu}_2(\text{OH})_3\text{NO}_3$, *Phys. Rev. B* **106**, 085119 (2022).
- [25] A. Orendáčová, E. Čížmár, L. Sedláková, J. Hanko, M. Kajňaková, M. Orendáč, A. Feher, J. S. Xia, L. Yin, D. M. Pajeroski, M. W. Meisel, V. Zeleňák, S. Zvyagin, and J. Wosnitza, Interplay of frustration and magnetic field in the two-dimensional quantum antiferromagnet $\text{Cu}(\text{tn})\text{Cl}_2$, *Phys. Rev. B* **80**, 144418 (2009).
- [26] V. Zeleňák, A. Orendáčová, I. Císařová, J. Černák, O. V. Kravchyna, J.-H. Park, M. Orendáč, A. G. Anders, A. Feher, and M. W. Meisel, Magneto-structural correlations in $\text{Cu}(\text{tn})\text{Cl}_2(\text{tn})1,3$ -diaminopropane): Two-dimensional spatially anisotropic triangular magnet formed by hydrogen bonds, *Inorg. Chem.* **45**, 1774 (2006).
- [27] L. Baranová, A. Orendáčová, E. Čížmár, R. Tarasenko, V. Tkáč, A. Feher, and M. Orendáč, Fingerprints of field-induced Berezinskii–Kosterlitz–Thouless transition in quasi-two-dimensional $S = 1/2$ Heisenberg magnets $\text{Cu}(\text{en})(\text{H}_2\text{O})_2\text{SO}_4$ and $\text{Cu}(\text{tn})\text{Cl}_2$, *J. Magn. Magn. Mater.* **404**, 53 (2016).
- [28] C. A. Corrêa, M. Poupon, V. Petříček, R. Tarasenko, M. Mihálik, D. Legut, U. D. Wdowik, and A. Orendáčová, Phase transformation in quasi-two-dimensional quantum antiferromagnet $\text{Cu}(\text{tn})\text{Cl}_2$ ($\text{tn}=1,3$ -diaminopropane), *J. Phys. Chem. C* **126**, 14573 (2022).
- [29] D. Harvey and C. J. L. Lock, Dichloro(ethylenediamine) copper(II), *Acta Crystallogr., Sect. C: Struct. Chem.* **42**, 799 (1986).
- [30] M. Zabel, V. I. Pawlowski, and A. L. Poznyak, Phase transition in dichloro(ethylenediamine) copper(II) crystals $[(\text{En})\text{CuCl}(\mu_3\text{-Cl})]$ and their structure, *J. Struct. Chem.* **47**, 585 (2006).
- [31] F. L. Pratt, WIMDA: A muon data analysis program for the Windows PC, *Phys. B (Amsterdam, Neth.)* **289**, 710 (2000).
- [32] P. Giannozzi, S. Baroni, N. Bonini, M. Calandra, R. Car, C. Cavazzoni, D. Ceresoli, G. L. Chiarotti, M. Cococcioni, I. Dabo *et al.*, QUANTUM ESPRESSO: A modular and open-source software project for quantum simulations of materials, *J. Phys.: Condens. Matter* **21**, 395502 (2009).
- [33] P. Giannozzi, O. Andreussi, T. Brumme, O. Bunau, M. B. Nardelli, M. Calandra, R. Car, C. Cavazzoni, D. Ceresoli, M. Cococcioni *et al.*, Advanced capabilities for materials modelling with QUANTUM ESPRESSO, *J. Phys.: Condens. Matter* **29**, 465901 (2017).
- [34] P. E. Blöchl, Projector augmented-wave method, *Phys. Rev. B* **50**, 17953 (1994).
- [35] J. P. Perdew, K. Burke, and M. Ernzerhof, Generalized gradient approximation made simple, *Phys. Rev. Lett.* **77**, 3865 (1996).

- [36] S. Grimme, J. Antony, S. Ehrlich, and H. Krieg, A consistent and accurate *ab initio* parametrization of density functional dispersion correction (DFT-D) for the 94 elements H-Pu, *J. Chem. Phys.* **132**, 154104 (2010).
- [37] N. Marzari, A. A. Mostofi, J. R. Yates, I. Souza, and D. Vanderbilt, Maximally localized Wannier functions: Theory and applications, *Rev. Mod. Phys.* **84**, 1419 (2012).
- [38] G. Pizzi, V. Vitale, R. Arita, S. Blügel, F. Freimuth, G. Géranton, M. Gibertini, D. Gresch, Ch. Johnson, T. Koretsune *et al.*, Wannier90 as a community code: New features and applications, *J. Phys.: Condens. Matter* **32**, 165902 (2020).
- [39] A. A. Mostofi, J. R. Yates, G. Pizzi, Y. S. Lee, I. Souza, D. Vanderbilt, and N. Marzari, An updated version of WANNIER90: A tool for obtaining maximally-localised Wannier functions, *Comput. Phys. Commun.* **185**, 2309 (2014).
- [40] X. He, N. Helbig, M. J. Verstraete, and E. Bousquet, TB2J: A python package for computing magnetic interaction parameters, *Comput. Phys. Commun.* **264**, 107938 (2021).
- [41] A. I. Liechtenstein, M. I. Katsnelson, V. P. Antropov, and V. A. Gubanov, Local spin density functional approach to the theory of exchange interactions in ferromagnetic metals and alloys, *J. Magn. Magn. Mater.* **67**, 65 (1987).
- [42] Dm. M. Korotin, V. V. Mazurenko, V. I. Anisimov, and S. V. Streltsov, Calculation of exchange constants of the Heisenberg model in plane-wave-based methods using the Green's function approach, *Phys. Rev. B* **91**, 224405 (2015).
- [43] See Supplemental Material at <http://link.aps.org/supplemental/10.1103/PhysRevB.108.214432> for concerning spin anisotropies and DFT calculations of exchange couplings for several antiferromagnetic configurations, the complete symmetry analysis of spin interactions in Cu(tn)Cl₂ was performed within the Pnma space group using a two-sublattice model and low-energy approximation, the ground-state spin configurations were calculated depending on the hierarchy of spin anisotropies, interlayer coupling, and orientation of magnetic field. The Supplemental Material also contains Refs. [44,45].
- [44] N. Papanicolaou, Antiferromagnetic domain walls, *Phys. Rev. B* **51**, 15062 (1995).
- [45] J. Chovan and N. Papanicolaou, Low-frequency spin dynamics in the orthorhombic phase of La₂CuO₄, *Eur. Phys. J. B* **17**, 581 (2000).
- [46] A. W. Sandvik, Stochastic series expansion method with operator-loop update, *Phys. Rev. B* **59**, R14157(R) (1999).
- [47] B. Bauer, L. D. Carr, H. G. Evertz, A. Feiguin, J. Freire, S. Fuchs, L. Gamper, J. Gukelberger, E. Gull, S. Guertler *et al.*, The ALPS project release 2.0: Open source software for strongly correlated systems, *J. Stat. Mech.: Theor. Exp.* (2011) P05001.
- [48] L. Lederová, A. Orendáčová, R. Tarasenko, K. Karl'ová, J. Strečka, A. Gendiar, M. Orendáč, and A. Feher, Interplay of magnetic field and interlayer coupling in the quasi-two-dimensional quantum magnet Cu(en)Cl₂: Realization of the spin-1/2 rectangular/zigzag square Heisenberg lattice, *Phys. Rev. B* **100**, 134416 (2019).
- [49] R. Tarasenko, L. Lederová, A. Orendáčová, M. Orendáč, and A. Feher, Experimental study of magneto-structural correlations in low-dimensional quantum magnets Cu(en)Cl₂ and Cu(tn)Cl₂, *Acta Phys. Pol., A* **133**, 420 (2018).
- [50] K. Sun, J. H. Cho, F. C. Chou, W. C. Lee, L. L. Miller, D. C. Johnston, Y. Hidaka, and T. Murakami, Heat capacity of single-crystal La₂CuO₄ and polycrystalline La_{2-x}Sr_xCuO₄ (0 ≤ x ≤ 0.20) from 110 to 600 K, *Phys. Rev. B* **43**, 239 (1991).
- [51] S. Chakravarty, B. I. Halperin, and D. R. Nelson, Low-temperature behavior of two-dimensional quantum antiferromagnets, *Phys. Rev. Lett.* **60**, 1057 (1988).
- [52] D. Ihle, C. Schindelin, A. Weiße, and H. Fehske, Magnetic order-disorder transition in the two-dimensional spatially anisotropic Heisenberg model at zero temperature, *Phys. Rev. B* **60**, 9240 (1999).
- [53] F.-J. Jiang, F. Kämpfer, and M. Nyfeler, Monte Carlo determination of the low-energy constants of a spin-1/2 Heisenberg model with spatial anisotropy, *Phys. Rev. B* **80**, 033104 (2009).
- [54] L. Lederová, A. Orendáčová, J. Chovan, J. Strečka, T. Verkholyak, R. Tarasenko, D. Legut, R. Sýkora, E. Čižmár, V. Tkáč *et al.*, Realization of a spin-1/2 spatially anisotropic square lattice in a quasi-two-dimensional quantum antiferromagnet Cu(en)(H₂O)₂SO₄, *Phys. Rev. B* **95**, 054436 (2017).
- [55] Y. Kohama, M. Jaime, O. E. Ayala-Valenzuela, R. D. McDonald, E. D. Mun, J. F. Corbey, and J. L. Manson, Field-induced XY and Ising ground states in a quasi-two-dimensional S = 1/2 Heisenberg antiferromagnet, *Phys. Rev. B* **84**, 184402 (2011).
- [56] K. Yu. Povarov, A. I. Smirnov, and C. P. Landee, Switching of anisotropy and phase diagram of the Heisenberg square-lattice S = 1/2 antiferromagnet Cu(pz)₂(ClO₄)₂, *Phys. Rev. B* **87**, 214402 (2013).
- [57] T. Radu, H. Wilhelm, V. Yushankhai, D. Kovrizhin, R. Coldea, Z. Tyliczynski, T. Lühmann, and F. Steglich, Bose-Einstein condensation of magnons in Cs₂CuCl₄, *Phys. Rev. Lett.* **95**, 127202 (2005).
- [58] R. Tarasenko, A. Orendáčová, E. Čižmár, M. Orendáč, I. Potočník, S. Zvyagin, and A. Feher, Spin anisotropy in Cu(tn)Cl₂: A quasi-two-dimensional S = 1/2 spatially anisotropic triangular-lattice antiferromagnet, *J. Phys.: Conf. Ser.* **903**, 012005 (2017).
- [59] P. Sengupta, C. D. Batista, R. D. McDonald, S. Cox, J. Singleton, L. Huang, T. P. Papageorgiou, O. Ignatchik, T. Herrmannsdörfer, J. L. Manson, J. A. Schlueter, K. A. Funk, and J. Wosnitzer, Nonmonotonic field dependence of the Néel temperature in the quasi-two-dimensional magnet [Cu(HF₂)(pyz)₂]BF₄, *Phys. Rev. B* **79**, 060409(R) (2009).
- [60] A. Cuccoli, T. Roscilde, V. Tognetti, R. Vaia, and P. Verrucchi, Quantum Monte Carlo study of S = 1/2 weakly anisotropic antiferromagnets on the square lattice, *Phys. Rev. B* **67**, 104414 (2003).
- [61] D. Opherden, N. Nizar, K. Richardson, J. C. Monroe, M. M. Turnbull, M. Polson, S. Vela, W. J. A. Blackmore, P. A. Goddard, J. Singleton *et al.*, Extremely well isolated two-dimensional spin-1/2 antiferromagnetic Heisenberg layers with a small exchange coupling in the molecular-based magnet CuPOF, *Phys. Rev. B* **102**, 064431 (2020).
- [62] E. S. Klyushina, J. Reuther, L. Weber, A. T. M. N. Islam, J. S. Lord, B. Klemke, M. Månsson, S. Wessel, and B. Lake, Signatures for Berezinskii-Kosterlitz-Thouless critical behavior in the planar antiferromagnet BaNi₂V₂O₈, *Phys. Rev. B* **104**, 064402 (2021).
- [63] R. Kadono, T. Matsuzaki, T. Yamazaki, S. R. Kretzman, and J. H. Brewer, Spin dynamics of the itinerant helimagnet MnSi

- studied by positive muon spin relaxation, *Phys. Rev. B* **42**, 6515 (1990).
- [64] J. R. Stewart and R. Cywinski, μ SR evidence for the spin-liquid-to-spin-glass transition in β -Mn $_{1-x}$ Al $_x$, *Phys. Rev. B* **59**, 4305 (1999).
- [65] R. Melzi, S. Aldrovandi, F. Tedoldi, P. Carretta, P. Millet, and F. Mila, Magnetic and thermodynamic properties of Li $_2$ VOSiO $_4$: A two-dimensional $S = 1/2$ frustrated antiferromagnet on a square lattice, *Phys. Rev. B* **64**, 024409 (2001).
- [66] A. H. Castro Neto and Daniel Hone, Doped planar quantum antiferromagnets with striped phases, *Phys. Rev. Lett.* **76**, 2165 (1996).
- [67] T. Pardini, R. R. P. Singh, A. Katanin, and O. P. Sushkov, Spin stiffness of the anisotropic Heisenberg model on the square lattice and a possible mechanism for pinning of the electronic liquid crystal direction in underdoped YBa $_2$ Cu $_3$ O $_{6.45}$, *Phys. Rev. B* **78**, 024439 (2008).
- [68] K. Kojima, A. Keren, G. M. Luke, B. Nachumi, W. D. Wu, Y. J. Uemura, M. Azuma, and M. Takano, Magnetic behavior of the 2-leg and 3-leg spin ladder cuprates Sr $_{n-1}$ Cu $_{n+1}$ O $_{2n}$, *Phys. Rev. Lett.* **74**, 2812 (1995).
- [69] Y. J. Uemura, A. Keren, K. Kojima, L. P. Le, G. M. Luke, W. D. Wu, Y. Ajiro, T. Asano, Y. Kuriyama, M. Mekata *et al.*, Spin fluctuations in frustrated kagomé lattice system SrCr $_8$ Ga $_4$ O $_{19}$ studied by muon spin relaxation, *Phys. Rev. Lett.* **73**, 3306 (1994).
- [70] W. Yao, Q. Huang, T. Xie, A. Podlesnyak, A. Brassington, C. Xing, R. S. D. Mudiyansele, H. Wang, Weiwei Xie, S. Zhang, M. Lee *et al.*, Continuous spin excitations in the three-dimensional frustrated magnet K $_2$ Ni $_2$ (SO $_4$) $_3$, *Phys. Rev. Lett.* **131**, 146701 (2023).
- [71] Z. Zhu, B. Pan, L. Nie, J. Ni, Y. Yang, C. Chen, C. Jiang, Y. Huang, E. Cheng, Y. Yu *et al.*, Fluctuating magnetic droplets immersed in a sea of quantum spin liquid, *Innovation* **4**, 100459 (2023).